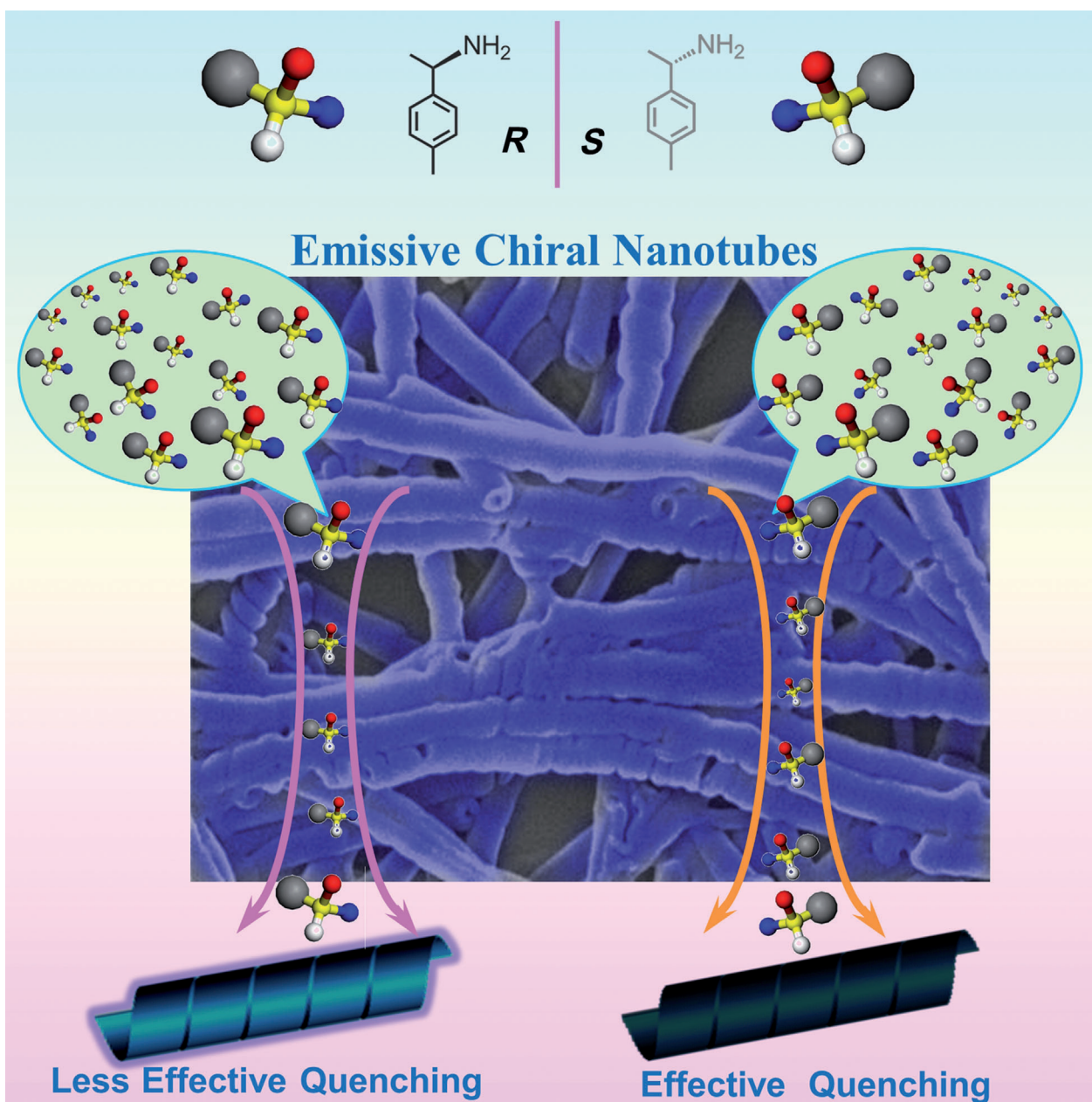


## Self-Assembly of $\pi$ -Conjugated Gelators into Emissive Chiral Nanotubes: Emission Enhancement and Chiral Detection

Xiufeng Wang, Pengfei Duan, and Minghua Liu\*<sup>[a]</sup>



**Abstract:** A series of new  $\pi$ -conjugated gelators that contain various aromatic rings (phenyl, naphthyl, 9-anthryl) and amphiphilic L-glutamide was designed, and their gel formation in organic solvents and self-assembled nanostructures was investigated. The gelators showed good gelation ability in various organic solvents that ranged from polar to nonpolar. Those gelator molecules

with small rings such as phenyl and naphthyl self-assembled into nanotube structures in most organic solvents and showed strong blue emission. However, the 9-anthryl derivative formed only a nanofiber structure in any organic

solvent, probably owing to the larger steric hindrance. All of these gels showed enhanced fluorescence in organogels. Furthermore, during the gel formation, the chirality at the L-glutamide moiety was transferred to the nanostructures, thus leading to the formation of chiral nanotubes. One of the nanotubes showed chiral recognition toward the chiral amines.

**Keywords:** amines • chirality • gels • nanotubes • self-assembly

## Introduction

One-dimensional nanotube structures have been receiving a great deal of attention in the fields of both materials chemistry and biological systems. As materials, the one-dimensional hollow nanostructures provide a special and confined space, and some unique properties or enhanced performances can be expected,<sup>[1]</sup> which could provide many interesting applications. In biological systems, bundled tubular structures on the nano- to microscale, such as axons of the sciatic nerve in the human body, function in the maintenance of cell structures or the transport of proteins or organelles in the cell,<sup>[2]</sup> which has encouraged many efforts to mimic these systems.

Since the 1990s, several kinds of nanotubes have been the subject of much attention. One is the carbon nanotube, which was initially observed by Iijima in 1991 and has attracted long and continuous interest owing to its unique electronic properties as well as its stability and various applications.<sup>[3]</sup> The second kind is self-assembled nanotubes based on peptides or various amphiphiles. The peptide nanotube (PNT), which was first reported by Ghadiri's group and self-assembled based on the rational design of oligopeptide,<sup>[4]</sup> has been extensively investigated, and applications of PNTs in drug delivery, biosensors, filters, and microelectronics have been proposed.<sup>[5]</sup> Organic or lipid nanotubes (ONT, LNT), which were generally self-assembled from various kinds of amphiphilic building blocks<sup>[6]</sup> such as phospholipids, bola-amphiphiles, glucolipids, amphiphilic metal complexes, and so on, provided an important type of soft nanomaterials in which diverse functions can be tailored. Since these two kinds of nanotube are generally self-assembled through noncovalent bonds, they provide the opportunity to tune their properties as well as their functions through molecular design.<sup>[7]</sup> Although a deeper understanding of the noncovalent bond and great efforts in the design

of the building motifs have been carried out, it still remains a great challenge to realize both structural and functional control.<sup>[8]</sup> The self-assembly of  $\pi$ -conjugated molecules provided one of the most convenient ways to meet such a challenge. Various  $\pi$ -conjugated molecules,<sup>[9]</sup> such as hexabenzocoronene (HBC), porphyrins, and  $\pi$ -conjugated oligomers, have been designed and widely used as building blocks in self-assembled architectures to prepare nanotubes, nanowires, and so forth. Despite these excellent examples of architectures,  $\pi$ -conjugated nanotubes<sup>[10]</sup> are still less investigated relative to nanofiber structures.<sup>[11]</sup> Furthermore, considering the structure and functions of the nanotube, chirality is also an important issue. Although many functional chiral nanotubes have been fabricated, their unique functions have not been extensively investigated. In this paper, we have developed a simple way to fabricate  $\pi$ -conjugated chiral nanotubes through gel formation and we have found a novel chiral recognition toward the chiral amine.

Relative to general amine detection, chiral amine detection has been deemed more difficult and challenging. Amine vapor is teratogenic, carcinogenic, and can be absorbed by the human body through the skin as well as the gastrointestinal and respiratory tract. Therefore the detection of various amines is very important. A unique enantioselective gelation in response to the chirality of a chiral amine was reported in the system of poly(phenylacetylene)-bearing cyclodextrin pendants.<sup>[12]</sup> Molecularly imprinted polymers can be used as fluorescent sensors for chiral amines.<sup>[13]</sup> In addition, a fluorescent sensor based on chiral trifluoromethyl ketone was developed to detect chiral diamine with high sensitivity and enantioselectivity by Pu's group.<sup>[14]</sup> In spite of these studies, however, no report has appeared on using functional  $\pi$ -conjugated nanotubes for enantioselective fluorescent recognition of chiral amines or chiral amine vapor.

Low-molecular-weight organogels provide numerous opportunities not only for gelling various organic solvents but also for the formation of nanostructures. Through the gel formation, relatively uniform nanostructured materials could be fabricated in large quantities. Although many of the nanostructures in the organogels were revealed to be fibrillar structures, other forms such as nanorods and nanotapes are frequently encountered.<sup>[15]</sup> Nanotubes are also one of the important structures that organogels can provide. Previously, we have realized the formation of chiral nanotubes

[a] X. Wang, Dr. P. Duan, Prof. Dr. M. Liu  
Beijing National Laboratory for Molecular Science  
CAS Key Laboratory of Colloid, Interface and  
Chemical Thermodynamics, Institute of Chemistry  
Chinese Academy of Sciences, Beijing, 100190 (China)  
Fax: (+86) 10-6256-9564  
E-mail: liumh@iccas.ac.cn

Supporting information for this article is available on the WWW  
under <http://dx.doi.org/10.1002/asia.201301518>.

and tuned their chirality by mixing different enantiomers of *N,N'*-bis(octadecyl)-*L*-glutamic diamide (LGAm) and *N,N'*-bis(octadecyl)-*D*-glutamic acid diamide (DGAm).<sup>[16a]</sup> The good gelation properties of *L*-glutamide made us wonder whether we could attach  $\pi$ -conjugated groups onto one end of this moiety and realize  $\pi$ -conjugated nanotubes. Our group has further designed several gelators that contain LGAm with different functional  $\pi$ -conjugated sections.<sup>[16]</sup> Although these gelators did not form a nanotube structure, they showed a multiresponsive chiroptical switch, universal nanotwists, chiral recognition of *L*-/*D*-tartaric acid, and so forth. In this experiment, we linked several simple aromatic rings of different sizes from phenyl, naphthyl, and anthryl to LGAm through amide bonds. Figure 1 shows the molecular

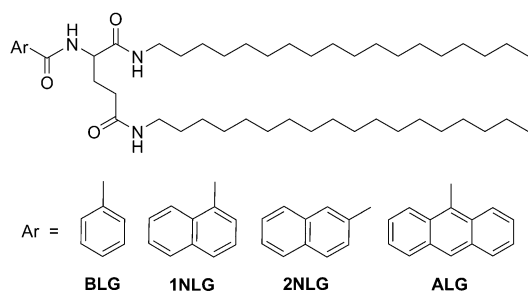


Figure 1. Molecular structures designed with different aromatic rings: phenyl, 1-naphthyl, 2-naphthyl, and 9-anthryl are called (from left to right) BLG, 1NLG, 2NLG, and ALG, respectively.

structures we designed. We have found that these molecules could gel many organic solvents that ranged from nonpolar to polar. In addition to the derivative with larger anthracene derivatives, those of the derivative with phenyl and naphthyl could form nanotube structures in many organic solvents. Relative to those  $\pi$ -conjugated nanotubes,<sup>[9–11]</sup> our derivatives are easily synthesized and with simpler  $\pi$ -conjugated aromatic rings. Upon gel formation, the fluorescence of the gel was significantly enhanced. However, the xerogels of these compounds are in a nanotube form, and were found to be sensitive to amine and could serve as an amine detector. Furthermore, since the gelator molecules have chiral centers, when they form organogels, their molecular chirality can be transferred to the supramolecular nanotube. Interestingly, when enantiomeric amine vapor was introduced to the nanotube, the nanotube showed excellent discrimination toward the derivatives, thus working as a chiral sensing system, although such recognition could not happen at a molecular level. Thus, through a simple molecular design, we have realized uniform nanotubes from 1NLG that can be used to detect chiral amine vapor.

### Organogelation: Solvent-Regulated Nanofibers and Nanotubes

The gel was fabricated in a general way. The solid was dispersed into a certain amount of organic solvent and heated

to the boiling point of the solvent. Then a transparent solution could be obtained. Upon cooling to room temperature, the solution became solidified. The gel formation was confirmed by the inverted test-tube method. Various organic solvents from polar to nonpolar ones were tested, as shown in Table 1. Compounds BLG, 1NLG, and 2NLG were able

Table 1. Gelation properties of BLG, 1NLG, 2NLG, and ALG in various organic solvents.

Solvent	BLG phase <sup>[a]</sup>	1NLG phase <sup>[a]</sup>	2NLG phase <sup>[a]</sup>	ALG phase <sup>[a]</sup>
toluene	TG (1.3)	TG (1.5)	TG (1.1)	TG (6.5)
DMSO	G (1.3)	G (1.4)	G (1.8)	G (12)
DMF	G (2.5)	G (2.3)	G (2.4)	G (4.8)
tetrahydrofuran	TG (6.0)	TG (6.0)	TG (6.0)	S
acetonitrile	G (3.0)	G (3.0)	G (3.0)	PG
ethyl acetate	G (2.6)	G (2.5)	G (2.4)	P
ethanol	G (2.0)	G (5.0)	G (5.0)	P
<i>n</i> -hexane	TG (2.4)	TG (2.5)	TG (2.5)	TG (3.2)
cyclohexane	TG (2.6)	TG (2.5)	TG (2.5)	TG (3.3)

[a] G = gel; TG = transparent gel; PG = partial gel; P = precipitate; S = solution. For gels, the minimum gelation concentrations, CGC [mgmL<sup>-1</sup>], at room temperature are shown in parentheses.

to gel the various organic solvents tested. Except for the transparent and colorless gel that formed in toluene and cyclohexane, translucent or white gels were essentially observed in polar solvents. Depending on the solvent, the critical gelation concentration (CGC) is somewhat different, and the lowest CGC was obtained in toluene. Whereas compounds BLG, 1NLG, and 2NLG were able to gel various organic solvents, ALG could only gel a few kinds of solvents. In addition, its CGC increased significantly. Similar to the other three compounds, transparent yellow gels were obtained in toluene, *n*-hexane, and cyclohexane, and translucent yellow gels only formed in DMSO and DMF.

The organogels in various organic solvents were fabricated into xerogels by evaporating the solvents, and their morphologies were investigated by scanning and transmission electron microscopy (SEM and TEM). The polarity of the solvents affected the assembly of gelators. In nonpolar solvents, such as toluene, *n*-hexane, and cyclohexane, the gelators of BLG, 1NLG, and 2NLG can all assemble into random nanofibers, which became entangled with each other to immobilize the solvents (see the Supporting Information). In strong polar solvents such as acetonitrile, DMF, and DMSO, BLG assembled into nanotube structures, whereas in other polar solvents, nanofibers were generally obtained. For 1NLG and 2NLG, nanotubes could be obtained in most polar solvents such as ethanol, THF, acetone, ethyl acetate, acetonitrile, DMF, and DMSO. When the head group was changed to a large aromatic anthryl, no nanotube was observed from any ALG organogel (see the Supporting Information). Instead, only nanofibers or other random structures could be obtained. SEM images of nanotubes in various polar solvents are shown in the Supporting Information. The smooth surface and the straight and open-

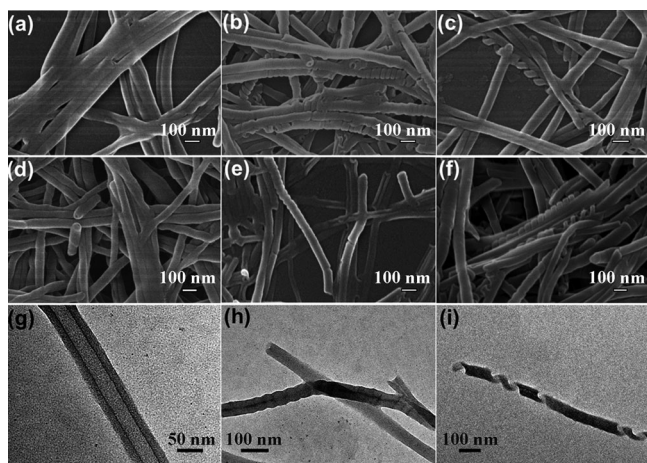


Figure 2. SEM images of a DMSO gel of a) BLG, b) 1NLG, c) 2NLG; and acetonitrile gel of d) BLG, e) 1NLG, f) 2NLG. TEM images of g) a BLG gel in DMSO, h) a 1NLG gel in DMSO, and i) 2NLG in acetonitrile, separately.

ended features revealed a tubular structure. Then we chose DMSO and acetonitrile as representative solvents to study their structures in detail. Figure 2 shows the SEM and TEM images for some of the organized structures.

The SEM revealed the nanotube structures for the three gelators. The high-quality SEM image of the assemblies indicated the formation of nanotubes with a high aspect ratio and uniform diameters for 1NLG and 2NLG. Although the tubular structure is not clear for BLG, the open mouth of the nanotube can be clearly seen in the SEM image. It is further evident that the nanotubes are rolled from the nanobelt, as a distinct helix turn can be seen in Figure 2b,c,e,f for 1NLG and 2NLG. The tubular structures were solidly confirmed by TEM, in which two dark parallel ribbons separated by a light center (Figure 2g–i) can be seen. The diameter of the BLG nanotube is approximately  $(63 \pm 2)$  nm, 1NLG is  $(50 \pm 2)$  nm, and 2NLG is  $(50 \pm 2)$  nm.

### Gelation-Induced Enhancement of Fluorescence Emission

Upon gel formation, these compounds showed strong blue emission upon UV irradiation. The luminescence spectra of the gels in various solvents were investigated. The gel 2NLG showed the strongest emission, and BLG was the worst at the same concentration in DMSO solvent. Figure 3 shows the fluorescence spectra of the compounds in solution and the gel state. For BLG gel, a weak blue emission was observed with an excitation of 270 nm, although there is no fluorescence in the solution state.

For compound 1NLG, the fluid solution in DMSO showed a very weak fluorescence under illumination at 254 nm UV light. The concentration-dependent fluorescence spectra of 1NLG in solution were also measured and are shown in the Supporting Information. Before the gel formation, the emission peak at 339 nm redshifted to 344 nm, and the intensity increased as the concentration increased. Upon

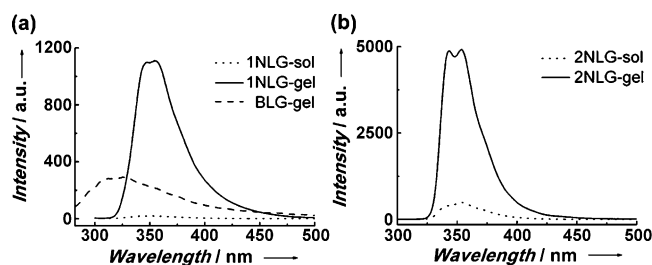


Figure 3. The fluorescence spectra of a) a solution and gel of 1NLG and b) 2NLG in DMSO. The fluorescence intensity of BLG (dashed line) is twenty times the original data.

gel formation, the fluorescence emission was significantly enhanced; it appeared at 344 and 356 nm upon excitation at 290 nm. The emission intensity of 1NLG gel increased by more than fifty times than that of the solution state, which could be ascribed to the aggregation-induced enhanced emission.<sup>[17]</sup> Such an unusual phenomenon has been frequently observed in the organogel as well.<sup>[18]</sup> In the present gel, the aggregation-induced enhanced emission (AIEE) was attributed to inhibition of intramolecular rotation in the gel state and the intermolecular stacking. The emission of the gel is observed at longer wavelengths than in solution, which suggests that 1NLG piled up tightly in a J-aggregation fashion. In J aggregation, the lower excited-state energy level formed by dipole–dipole interactions is an allowed transition to the ground state, which favors aggregate emission.<sup>[18e]</sup> As a result, the fluorescence emission of the gel is much stronger than that of the monomer. And the result of 2NLG is similar to that of 1NLG (Figure 3b).

It has been further observed that the organic solvents also have a strong effect on the fluorescence through either their emission band or the intensity. Figure 4 shows the fluorescence spectra of various organogels. As shown in Figure 4a, the emission spectra of BLG gels vary with the solvents, which range from 287 (toluene) to 327 nm (DMSO). The

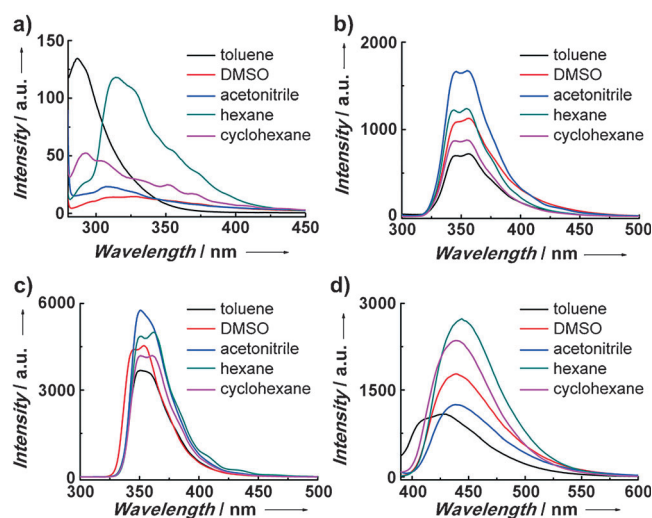


Figure 4. The fluorescence spectra of a) BLG, b) 1NLG, c) 2NLG, and d) ALG in various solvents.

fluorescence of 1NLG gels in various organic solvents indicated that there are two clear peaks at around 345 and 355 nm in most solvents. The 2NLG gels showed different intensities in relation to the polarity of the solvents. The peaks of nonpolar solvents such as toluene, *n*-hexane, and cyclohexane are at 351 and 362 nm, which become clearly redshifted relative to the polar solvents at 344 and 354 nm or so. In addition, the gels in nonpolar solvents are much stronger than those in polar solvents. For ALG, the fluorescence spectra are bound up with the solvents used, and the peak range is from 415 to 444 nm (shown in Figure 4d).

### Analysis of Organogel Driving Forces

To further characterize the gel formation and their driving forces, FTIR and XRD were measured on the xerogels. Figure 5a,b show the FTIR spectra and XRD patterns of the xerogels. We chose the typical assembly of nanotubes and focused on the assembly of BLG, 1NLG, and 2NLG in DMSO. In the FTIR spectra, characteristic vibration bands

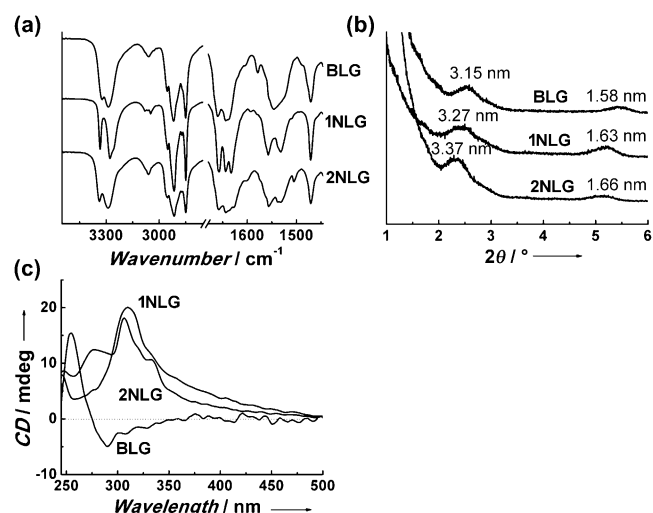


Figure 5. a) FTIR spectra and b) the XRD patterns of the BLG, 1NLG, and 2NLG xerogels and c) CD spectra of the corresponding gels in DMSO.

are observed clearly. The appearance of an N–H stretching vibration band around 3300 cm<sup>-1</sup> indicated the formation of the hydrogen bond. The two splits are assigned to two kinds of N–H bond; one kind is adjacent to the aromatic ring, and the other one links to the long alkyl chain. All the amide I and amide II bands appeared at around 1659–1630 and 1557–1532 cm<sup>-1</sup>, which indicates that both C=O and N–H are in the hydrogen-bonded form. At the same time, there are different degrees of splits in the amide I band at 1658 and 1644 cm<sup>-1</sup> with a shoulder at 1636 cm<sup>-1</sup> for BLG; 1658, 1644, and 1633 cm<sup>-1</sup> for 1NLG; and 1658, 1644, and 1628 cm<sup>-1</sup> for 2NLG, which suggest the existence of three kinds of amine bond. The asymmetric and symmetric stretching vibrations of CH<sub>2</sub> always appear at 2916 and 2849 cm<sup>-1</sup>, respectively, which suggests the alkyl chains

packed in an all-*trans* zigzag conformation.<sup>[19]</sup> The FTIR spectral features indicate that multiple hydrogen bonds between head groups together with the closely packed tails are the driving force for the formation of multi-bilayers and supramolecular nanotubes. In addition, the amide I and amide II bands of 1NLG/2NLG were a little different from BLG; they split clearer than BLG and appeared as three kinds of amide groups, thereby revealing that 1NLG/2NLG molecules arranged in a more orderly fashion. For 1NLG and 2NLG,  $\nu_{\text{as}}(\text{NH}_2)$  stretching frequencies move to a larger wavenumber, and  $\nu(\text{C}=\text{O})$  stretching frequencies moved to a lower one, which indicated the presence of stronger hydrogen bonds than BLG.<sup>[20]</sup>

X-ray diffraction measurements were performed to gain further insights into the different structural features. Then we chose DMSO and acetonitrile as representative polar solvents to further disclose the structures of the nanotubes, whereas toluene represents the nonpolar solvents for nanofiber structures (shown in Figure 5b and the Supporting Information). Well-defined diffraction patterns were observed in the xerogels from different gelling solvents. The two  $\theta$  values appeared at 2.53 and 5.41° for the BLG xerogel, at 2.54 and 5.27° for 1NLG, and 2.42 and 5.18° for 2NLG, respectively. The layer distance is estimated and listed in Figure 5b according to Bragg's equation. The *d*-spacing ratio is about 1:0.5, which was consistent with the lamellar structure. The value of the layer distance is less than twice the molecular dimension but larger than a single extended one, which suggests that BLG or NLG formed bilayer structures with interdigitation of the alkyl chain.<sup>[21]</sup> On the basis of the XRD pattern, the *d*-spacing value of 2NLG is larger than that of 1NLG, and the value for BLG is the smallest one. This is concordant with the single extended molecule length, which results from the different steric hindrance of the aromatic head group. In nonpolar solvents, the bilayer structures then stack to form nanofibers. In polar solvents, such as DMSO and acetonitrile, the bilayer structures further rolled into helices and then formed nanotubes,<sup>[22]</sup> as illustrated in Figure 7. By taking BLG gel in DMSO as an example, 3.15 nm corresponds to the *d*-spacing value of BLG in a bilayer structure. The wall thickness of the nanotubes is around 16 nm, as revealed by the TEM image in Figure 2g, therefore it can be inferred that the nanotubes were rolled up from 5 bilayers or orderly accumulated multiple bilayers. A similar lamellar structure and FTIR spectrum for ALG xerogel from DMSO are shown in the Supporting Information.

### Chirality of the Nanotube and Chiral Sensing

Since the gelator molecules have chiral centers, we measured the circular dichroism (CD) spectra of the organogels. As seen in Figure 5c, the CD spectrum of the BLG organogel in DMSO exhibits a negative band at 291 nm and a positive band at 254 nm, with a crossover at around 274 nm. For 1NLG and 2NLG, there are clear positive signals, which is in accordance with its adsorption band and indicates that

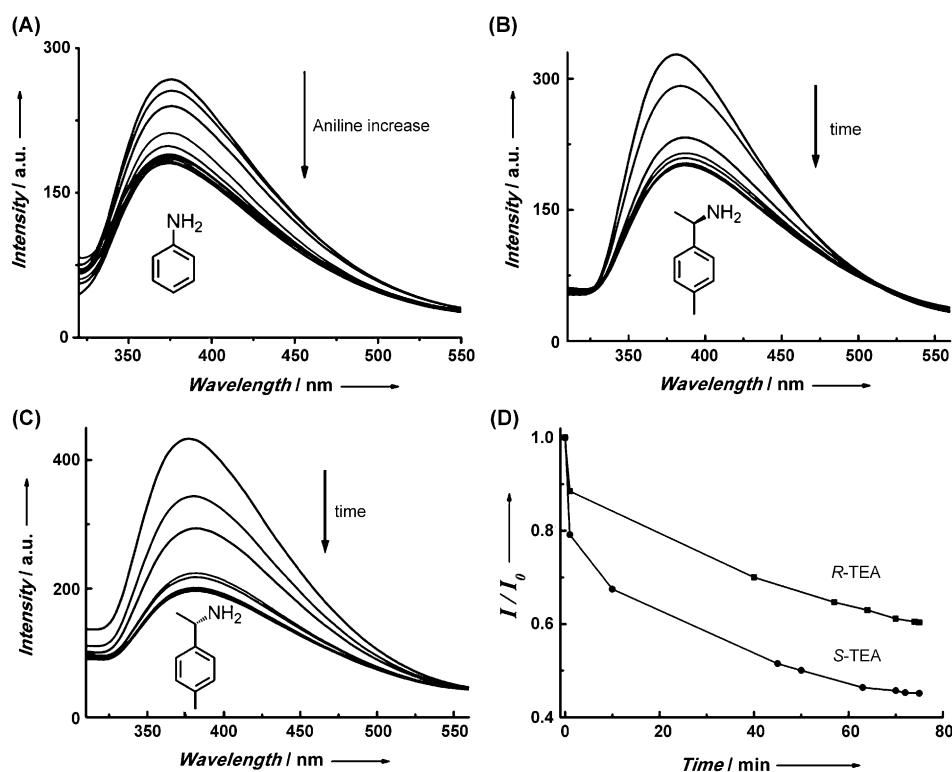


Figure 6. The fluorescence spectra of the 1NLG film in acetonitrile: A) exposure to the vapor of aniline; the intensity decreases as the volume of aniline vapor increases. Exposure to the vapor of chiral amine: B) (*R*)-TEA and C) (*S*)-TEA versus time. D) Fluorescence quenching efficiency of the 1NLG film by adding chiral amine versus time (from 0 to 75 min).

the structure was chiral. As has been noted before, 1NLG and 2NLG assemble into helical nanotubes with left-hand chirality in Figure 2b,c,e,f. On the basis of these CD spectra and the above SEM observation, it is clear that the chirality that is localized in the *L*-glutamide transferred to the whole assemblies during the gel formation.

Since these nanotubes showed strong emission, they were further used to test if these nanotubes can be used to detect amines. Aniline, owing to its low saturated vapor (880 ppm) among other organic amines, is a commonly examined organic amine.<sup>[23]</sup> Since aniline is aromatic, it is expected that the aromatic ring together with the electron-donor amino group could extinguish the fluorescence from the naphthyl ring in both 1NLG and 2NLG. Therefore, the nanotube films of both the compounds were prepared by casting a hot solution of 1NLG or 2NLG in acetonitrile onto a clean quartz plate. When the solvent volatilized completely, a thin film composed of the nanotube structures of either 1NLG or 2NLG was fabricated. These films were subsequently used to detect aniline vapor. The fluorescence emission spectra at different diluted vapor pressures were measured upon exposure to the vapor of aniline. Different vapor pressures were acquired by the injection of different volumes of saturated aniline vapor into the 10 mm sealed quartz cuvette with a cushion and screw cap.

In Figure 6A it can clearly be seen that the fluorescence is quenched. The intensity of the 1NLG fluorescence decreases

gradually as the volume of aniline vapor increases. The volume of the injected saturated aniline vapor was 20, 60, 100, 200, 300, 400, 500, 600, 800, and 1000  $\mu$ L in turn. Because the volume of the sealed quartz cuvette is 4.6 mL, the aniline converted into vapor pressure is 3.8, 7.6, 19.1, 38.3, 57.4, 76.5, 95.7, 114.8, 153, and 191 ppm. The film of 2NLG showed a similar fluorescence quenching phenomenon (Supporting Information). We have also investigated the effect of the different nanostructures on the detection of aniline. The films fabricated from toluene and acetonitrile gave nanofibers and nanotubes, respectively. The fluorescence results of the different nanostructures on exposure to aniline are shown in the Supporting Information. For the 1NLG film, it was observed that the nanotube showed a rapid decrease in fluorescence in response to the aniline vapor, but it was nearly the

same for 2NLG, which might be owing to the larger steric hindrance in 1NLG. However, in any case, the nanofiber structure exhibited a larger decrease of fluorescence at a higher vapor pressure.

In our study, chiral organic amines (*R*)-(+)-1-(*p*-tolyl)ethylamine and (*S*)-(–)-1-(*p*-tolyl)ethylamine ((*R*)-TEA and (*S*)-TEA) were tested too. The saturated vapor pressure of 1-(*p*-tolyl)ethylamine (TEA) is 279 ppm, which is lower than that of aniline. The fluorescence spectra were obtained in the following way. First, the cast film was sealed in a quartz cuvette. Then saturated (*R*)- or (*S*)-TEA vapor (1 mL) was injected into the cuvette. Figure 6B,C shows the change in fluorescence as a function of time. The fluorescence of the films was quenched by the chiral TEA and became saturated at 75 min. We compared the degree of the fluorescence quenching by the chiral amines and the  $I/I_0$  values in the equilibrium. No clear differences appeared in the cast films of 1NLG-toluene, 2NLG-toluene, 2NLG-acetonitrile, ALG-toluene, and ALG-acetonitrile, as shown in the Supporting Information. Interestingly, the result of 1NLG-acetonitrile, which is a nanotube structure, showed interesting results. When (*R*)-TEA was detected,  $I/I_0$  is about 0.60; this value changed to 0.43 when the *S* enantiomer was used. This indicated that during the interaction of the TEA enantiomer with the 1NLG nanotube, (*S*)-TEA is more favorable, which might be due to their chirality match.

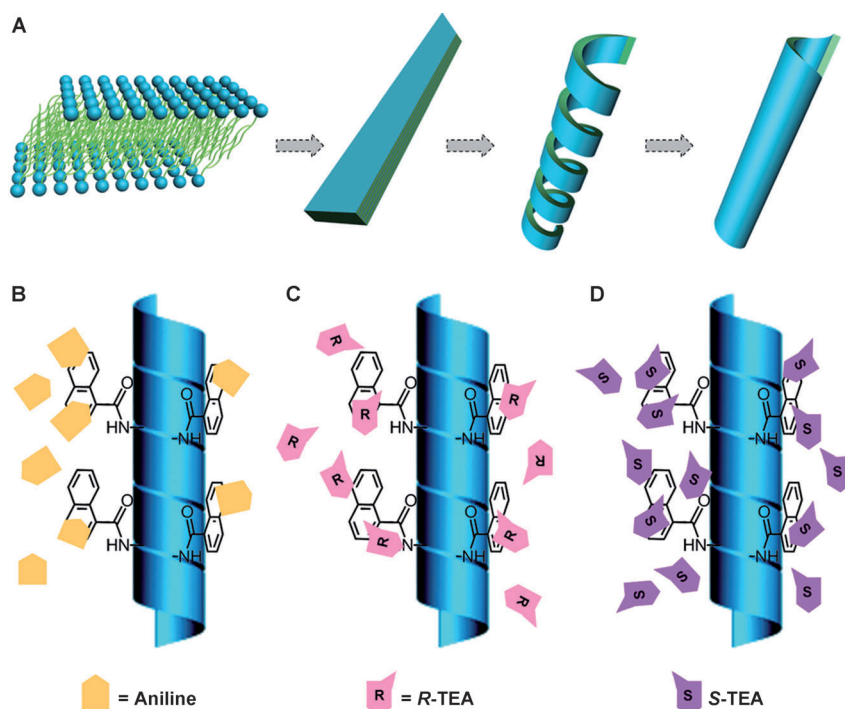


Figure 7. Illustration of A) nanotube formation. By taking 1NLG nanotubes as an example, the detection of aniline using B) 1NLG nanotubes, and 1NLG nanotube detection of chiral amine: C) *R* enantiomer and D) *S* enantiomer. The 1NLG nanotube favors the *S* enantiomer and disfavors the *R* enantiomer.

By combining the above data, the formation of nanotubes and nanofibers can be illustrated as in Figure 7. In strong polar solvents, BLG, 1NLG, and 2NLG molecules first formed a bilayer structure with interdigitated aliphatic tails. Then multiple bilayer structures were stacked into nanobelts. To reduce the large surface energy, the nanobelts were further rolled into helical structures owing to the chiral nature of the layered structure. Finally, these gelator molecules assembled into a nanotube structure. It is noteworthy that, to roll into nanotubes, the head group should not be too big. When ALG was used, the larger steric hindrance of the head group prevented its rolling and could only yield a fibrous structure.

Both nanofiber and nanotube structures of 1NLG and 2NLG can be used to detect aniline. Therefore, we propose a mechanism for the fluorescence sensing of gaseous amines, which is shown in Figure 7B. By taking 1NLG nanotubes obtained from acetonitrile as an example, aniline molecules can adsorb on the surface of the nanostructure by means of  $\pi$ - $\pi$  interactions between aniline and naphthyl. The other aromatic ring exhibits similar properties. This indicates that the gelators as electron-accepting materials are suitable for sensing electron-rich compounds such as organic amines. Similar to aniline detection, chiral organic amines that contain aromatic rings were also tested. On the basis of the results shown in Figure 6D, a 1NLG-acetonitrile cast film showed a distinct decrease in the fluorescence between (*R*)-TEA and (*S*)-TEA. This is directly linked to the nanostructure and the steric hindrance effect of the gelator. As a com-

parison, the sensing performances of other kinds of film toward chiral amines were also investigated. For the same 1NLG gelator, when the structure is a nanofiber, the fluorescence quenching with different enantiomers is nearly the same. The enantiomers were not distinguished from each other even with a different gelator with the same nanostructure. This further indicated that, in addition to the steric hindrance and the supramolecular chirality in the nanostructures, the curvature of the nanotube might also play an important role, which would make (*S*)-TEA more likely to access the nanotube, as illustrated in Figure 7C,D.

## Conclusion

The self-assembly of gelators with a  $\pi$ -conjugated aromatic ring was investigated in various organic solvents. The compounds with small rings such as phenyl and naphthyl can self-assemble into uniform nanotubes in many polar solvents, whereas they formed nanofiber structures in some nonpolar solvents. With its large steric hindrance, the 9-anthryl derivative could only form a nanofiber structure. Upon gel formation, the organogels exhibited clear fluorescence enhancement with blue emission. During the gel formation, the molecular chirality was transferred to the chromophores and the subsequent nanostructures. Strong CD signals were detected in the organogels. Furthermore, the helical nanotubes of 1NLG and 2NLG show the same left-handed chirality. Combined with enhanced fluorescence and supramolecular chirality, the film composed of the nanostructures by means of gelation was used to sense organic amines. Remarkably, the nanotube film of 1NLG showed enantioselectivity toward enantiomeric (*R*)- and (*S*)-1-(*p*-tolyl)ethanamine, in which the latter was favored.

## Experimental Section

### Materials

Compounds (*R*)- and (*S*)-1-(*p*-tolyl)ethanamine were purchased from TCI and used as received. The remaining chemicals and solvents were purchased from Beijing Chemical Reagent Industry. The  $\pi$ -conjugated gelators (BLG, 1NLG, 2NLG, and ALG) were synthesized as follows.

### Synthesis of the Aromatic L-Glutamic Lipid (BLG, INLG, 2NLG, and ALG)

The synthesis of *N,N'*-bis(octadecyl)-L-glutamic diamide (LGA) was reported previously.<sup>[16a]</sup>

#### Gelator BLG

LGA (0.85 g, 1.3 mmol) was dispersed in dichloromethane (40 mL) and stirred for 30 min. Benzoyl chloride (0.5 mL, 4.3 mmol) was dissolved in dichloromethane (20 mL) in a dropping funnel. Then the chloride was dropped into the above mixture and stirred at 0°C overnight. After that, the solvent was removed by rotary evaporation and a light yellow solid was obtained. The crude product was dissolved in THF (10 mL) and poured into an aqueous saturated solution of NaHCO<sub>3</sub> (300 mL). After filtration, the product was purified by recrystallization in ethanol to give a white solid (0.84 g, 85.7%). <sup>1</sup>H NMR (CDCl<sub>3</sub>, 400 Hz): δ = 0.86–0.89 (t, 6H; CH<sub>3</sub>), 1.25 (m, 60H; CH<sub>2</sub>), 1.50–1.53 (m, 4H; CH<sub>2</sub>), 1.85 (s, 1H; NH), 2.19–2.28 (q, 2H; CH<sub>2</sub>), 2.51–2.63 (m, 2H; CH<sub>2</sub>), 3.24–3.30 (m, 4H; CH<sub>2</sub>), 3.43–3.47 (t, 1H; NH), 4.58 (s, 1H; CH), 7.26–7.47 (m, 2H), 7.51–7.54 (m, 1H), 7.91–7.93 (d, 2H), 8.15 ppm (s, 1H; NH); MALDI-TOF MS: *m/z* calcd for C<sub>48</sub>H<sub>87</sub>N<sub>3</sub>O<sub>3</sub>: 753.7 [M]; found: 754.9 [M+Na]<sup>+</sup>, 776.9 [M+K]<sup>+</sup>, 792.9; elemental analysis calcd (%) for C<sub>48</sub>H<sub>87</sub>N<sub>3</sub>O<sub>3</sub>: C 76.44, H 11.63, N 6.36; found: C 76.16, H 11.80, N 5.61.

#### Gelator INLG

LGA (1.26 g, 1.94 mmol) was dispersed in dichloromethane (40 mL) and stirred for 30 min. 1-Naphthoyl chloride (0.7 g, 3.7 mmol) was dissolved in dichloromethane (20 mL) in a dropping funnel. The following procedure was the same as that for BLG. After filtration, the product was purified by recrystallization in ethanol to give a white solid (1.38 g, 85.9%). <sup>1</sup>H NMR (CDCl<sub>3</sub>, 400 Hz): δ = 0.86–0.89 (t, 6H; CH<sub>3</sub>), 1.24–1.30 (m, 60H; CH<sub>2</sub>), 1.40–1.52 (m, 4H; CH<sub>2</sub>), 2.17–2.27 (m, 2H; CH<sub>2</sub>), 2.50–2.63 (m, 2H; CH<sub>2</sub>), 3.28 (m, 4H; CH<sub>2</sub>), 4.70 (s, 1H; CH), 7.10 (s, 1H; NH), 7.26–7.47 (m, 1H), 7.49–7.57 (m, 3H), 7.69–7.71 (d, 1H), 7.86–7.88 (d, 1H), 7.93–7.95 (d, 1H), 8.34–8.36 ppm (d, 1H); MALDI-TOF MS: *m/z* calcd for C<sub>52</sub>H<sub>89</sub>N<sub>3</sub>O<sub>3</sub>: 803.7; found: 827.0 [M+Na]<sup>+</sup>; elemental analysis calcd (%) for C<sub>52</sub>H<sub>89</sub>N<sub>3</sub>O<sub>3</sub>: C 77.65, H 11.15, N 5.22; found: C 77.58, H 11.00, N 5.27.

#### Gelator 2NLG

LGA (1.3 g, 2 mmol) was dispersed in dichloromethane (40 mL) and stirred for 30 min. 2-Naphthoyl chloride (0.8 g, 4.2 mmol) was dissolved in dichloromethane (20 mL) in a dropping funnel. The following procedure was the same as that for BLG. After filtration, the product was purified by recrystallization in ethanol to give a white solid (1.45 g, 87.2%). <sup>1</sup>H NMR (CDCl<sub>3</sub>, 400 Hz): δ = 0.86–0.89 (t, 6H; CH<sub>3</sub>), 1.20–1.30 (m, 60H; CH<sub>2</sub>), 1.50–1.64 (m, 4H; CH<sub>2</sub>), 2.26–2.55 (m, 2H; CH<sub>2</sub>), 2.86 (m, 2H; CH<sub>2</sub>), 3.22–3.40 (m, 4H; CH<sub>2</sub>), 4.79 (s, 1H; CH), 7.26–7.60 (m, 2H), 7.86–7.92 (q, 2H), 7.97–7.99 (d, 1H), 8.03–8.05 (d, 1H), 8.64 ppm (s, 1H); MALDI-TOF MS: *m/z* calcd for C<sub>52</sub>H<sub>89</sub>N<sub>3</sub>O<sub>3</sub>: 803.7; found: 804.9 [M+Na]<sup>+</sup>, 827.0 [M+K]<sup>+</sup>, 843.0; elemental analysis calcd (%) for C<sub>52</sub>H<sub>89</sub>N<sub>3</sub>O<sub>3</sub>: C 77.65, H 11.15, N 5.22; found: C 78.28, H 10.29, N 4.76.

#### Gelator ALG

Anthracene-9-carboxylic acid (0.50 g, 2.25 mmol) was suspended in dry benzene (50 mL), and then SOCl<sub>2</sub> (3 mL) was added. The mixture was heated at reflux under strong stirring for 4 h. The solvent and the surplus SOCl<sub>2</sub> were then removed by rotary evaporation, and a dark brown solid, anthracene-9-carbonyl chloride, was obtained and used without further purification. LGA (1 g, 1.5 mmol) was dispersed in dichloromethane (40 mL) and stirred for 30 min. The obtained anthracene-9-carbonyl chloride was dissolved in dry CH<sub>2</sub>Cl<sub>2</sub> (30 mL) and was then added dropwise to the LGA solution within 30 min. The mixture was stirred for another 3 h at 0°C. After the reaction, the solution was washed with 0.01 M HCl (3 × 30 mL) and pure water (3 × 30 mL) and dried over magnesium sulfate under vacuum. The product was purified by recrystallization in ethanol to give a brown solid (0.77 g, 58.8%). <sup>1</sup>H NMR (CDCl<sub>3</sub>, 400 Hz): δ = 0.86–0.89 (t, 6H; CH<sub>3</sub>), 1.20–1.30 (m, 60H; CH<sub>2</sub>), 1.45–1.59 (m, 4H; CH<sub>2</sub>), 2.25–2.30 (m, 2H; CH<sub>2</sub>), 2.42–2.77 (m, 2H; CH<sub>2</sub>), 3.16–3.32 (m,

4H; CH<sub>2</sub>), 4.85–4.90 (q, 1H; CH), 6.09 (s, 1H), 7.38–7.30 (d, 1H), 7.45–7.51 (m, 4H), 8.00–9.02 (m, 4H), 8.48 ppm (s, 1H); MALDI-TOF MS: *m/z* calcd for C<sub>56</sub>H<sub>91</sub>N<sub>3</sub>O<sub>3</sub>: 853.7; found: 876.9 [M+Na]<sup>+</sup>; elemental analysis calcd (%) for C<sub>56</sub>H<sub>91</sub>N<sub>3</sub>O<sub>3</sub>: C 78.73, H 10.74, N 4.92; found: C 78.07, H 10.68, N 5.15.

#### General Methods

UV/Vis spectra were measured with a Hitachi U-3900 spectrophotometer. Fourier transform-infrared (FTIR) studies were performed with a JASCO FTIR-660 spectrometer. <sup>1</sup>H NMR spectra were recorded with a Bruker ARX400 (400 MHz) with Me<sub>4</sub>Si used as the internal standard and CDCl<sub>3</sub> for solvent. MALDI-TOF MS spectra were recorded with a BIFLEX III instrument. Elemental analyses were recorded with a Carlo-Erba-1106 instrument.

#### Circular Dichroism Spectroscopy

CD spectra were recorded with a JASCO J-810 CD spectrophotometer under a nitrogen atmosphere. Experiments were performed at room temperature in a quartz cell with a 0.1 mm path length over a range of 200–650 nm.

#### Fluorescence Spectroscopy Measurements

Fluorescence spectra were recorded with a Hitachi F-4600 spectrometer. The organogel was heated to a solution state, then transferred to a quartz cell with a 2 mm or 1 cm path length and heated to keep it transparent; the fluorescence was measured rapidly. Different solvents were used in the same way. After waiting for fifteen minutes, gelation took place completely, and then the fluorescence of the gel was measured. Fluorescence emission spectra of BLG were measured with excitation at 270 nm, INLG and 2NLG were measured with excitation at 290 nm, and ALG at 380 nm.

#### X-ray Diffraction Measurements

The organogel was spin-coated onto the glass substrate and dried under vacuum before measuring. XRD of the xerogels was performed with a Holland PANalytical X'Pert PRO MPD operating at 40 kV and 40 mA using CuK<sub>α</sub> radiation (λ = 1.5418 Å). The scan range (2θ) was from 1 to 6°.

#### SEM and TEM Measurements

The fully aged gel was cast onto single-crystal silica plates (Pt-coated) and carbon-coated Cu grids (unstained), and the trapped solvent in the gel was first evaporated under ambient conditions, then vacuum-dried for 12 h. After that, the performances were determined with a Hitachi S-4800 FESEM and JEOL TEM-2011 instrument operating at accelerating voltages of 10 and 200 kV, respectively.

#### Preparation of Organic Gels for Analysis

Different solvents (1 mL) were added to BLG, INLG, or 2NLG (3 mg) in a 5 mL vial, then the mixture was heated until the entire solid dissolved into a transparent solution. After standing at room temperature, the self-supporting organogel was usually complete within 10 to 30 min. Samples for SEM, TEM, UV/Vis, fluorescence, and CD studies were prepared without any dilution.

#### Fabrication of Cast Film

By taking the cast film of NLG nanotubes as an example, the samples of INLG and 2NLG (3.0 mg) were weighed separately in a 5 mL vial. Acetonitrile (1 mL) was added to the vial. The white solid sample was heated until it dissolved, and a transparent solution was obtained. The hot solution was cast into a clean quartz plate, and after the solvent evaporation was complete, a nanotube film was obtained. The structure of the film was determined by SEM, and many nanotubes were observed. Other cast films were prepared by following the same method.

## Fluorescence Measurement by Aniline Vapor

The fluorescence of aniline vapor with different concentrations was monitored following a method reported by Zang et al.<sup>[23a]</sup> The saturated vapor of aniline was achieved in a sealed serum bottle (25 mL). Before use the bottle was sealed overnight to attain a saturated vapor inside it. The cast film was measured inside a 10 mm sealed quartz cuvette with cushion and screw cap. The actual measured volume of the sealed quartz cuvette was 4.6 mL. Fluorescence quenching with different vapor pressures of aniline was performed in the cuvette. A small volume of the saturated vapor of aniline was immediately injected into the sealed cuvette by using a microsyringe to achieve the diluted vapor. After stabilizing for 120 s, the fluorescence of the film was measured. Throughout the whole measurement process, the cast film was kept immobile to guarantee that the fluorescence was measured at the same point and to ensure the accuracy and comparability of the monitoring data.

## Acknowledgements

We gratefully acknowledge funding of this research by the Basic Research Development Program (2013CB834504) and the National Natural Science Foundation of China (grant nos. 91027042, 21021003, and 21227802).

- [1] E. Gazit, *Chem. Soc. Rev.* **2007**, *36*, 1263–1269.
- [2] C. Conde, A. Caceres, *Nat. Rev. Neurosci.* **2009**, *10*, 319–332.
- [3] J. N. Coleman, U. Khan, W. J. Blau, Y. K. Gun'ko, *Carbon* **2006**, *44*, 1624–1652.
- [4] M. R. Ghadiri, J. R. Granja, R. A. Milligan, D. E. McRee, N. Khazanovich, *Nature* **1993**, *366*, 324–327.
- [5] a) S. Scanlon, A. Aggeli, *Nano Today* **2008**, *3*, 22–30; b) R. J. Brea, C. Reiriz, J. R. Granja, *Chem. Soc. Rev.* **2010**, *39*, 1448–1456; c) H. X. Xu, A. K. Das, M. Horie, M. S. Shaik, A. M. Smith, Y. Luo, X. F. Lu, R. Collins, S. Y. Liem, A. M. Song, P. L. A. Popelier, M. L. Turner, P. Xiao, I. A. Kinloch, R. V. Uljin, *Nanoscale* **2010**, *2*, 960–966.
- [6] a) S. Svenson, P. B. Messersmith, *Langmuir* **1999**, *15*, 4464–4471; b) H. Shao, M. Gao, S. H. Kim, C. P. Jaronec, J. R. Parquette, *Chem. Eur. J.* **2011**, *17*, 12882–12885; c) J. H. Jung, Y. Do, Y. A. Lee, T. Shimizu, *Chem. Eur. J.* **2005**, *11*, 5538–5544; d) Q. Jin, L. Zhang, H. Cao, T. Wang, X. Zhu, J. Jiang, M. Liu, *Langmuir* **2011**, *27*, 13847–13853; e) Y. Tang, L. Zhou, J. Li, Q. Luo, X. Huang, P. Wu, Y. Wang, J. Xu, J. Shen, J. Liu, *Angew. Chem.* **2010**, *122*, 4012–4016; *Angew. Chem. Int. Ed.* **2010**, *49*, 3920–3924.
- [7] R. S. Devan, R. A. Patil, J. H. Lin, Y. R. Ma, *Adv. Funct. Mater.* **2012**, *22*, 3326–3370.
- [8] a) T. Shimizu, M. Masuda, H. Minamikawa, *Chem. Rev.* **2005**, *105*, 1401–1443; b) D. T. Bong, T. D. Clark, J. R. Granja, M. R. Ghadiri, *Angew. Chem.* **2001**, *113*, 1016–1041; *Angew. Chem. Int. Ed.* **2001**, *40*, 988–1011; c) R. Chapman, M. Danial, M. L. Koh, K. A. Jolliffe, S. Perrier, *Chem. Soc. Rev.* **2012**, *41*, 6023–6041; d) N. Kameta, H. Minamikawa, M. Masuda, *Soft Matter* **2011**, *7*, 4539.
- [9] a) W. Zhang, W. Jin, T. Fukushima, N. Ishii, T. Aida, *J. Am. Chem. Soc.* **2013**, *135*, 114–117; b) Z. Wang, C. J. Medforth, J. A. Shelnett, *J. Am. Chem. Soc.* **2004**, *126*, 16720–16721; c) H. B. Liu, J. L. Xu, Y. J. Li, Y. L. Li, *Acc. Chem. Res.* **2010**, *43*, 1496–1508; d) V. K. Praveen, S. S. Babu, C. Vijayakumar, R. Varghese, A. Ajayaghosh, *Bull. Chem. Soc. Jpn.* **2008**, *81*, 1196–1211; e) A. Ajayaghosh, C. Vi-jayakumar, R. Varghese, S. J. George, *Angew. Chem.* **2006**, *118*, 470–474; *Angew. Chem. Int. Ed.* **2006**, *45*, 456–460.
- [10] a) H. Shao, J. Seifert, N. C. Romano, M. Gao, J. J. Helmus, C. P. Jaronec, D. A. Modarelli, J. R. Parquette, *Angew. Chem.* **2010**, *122*, 7854–7857; *Angew. Chem. Int. Ed.* **2010**, *49*, 7688–7691; b) Y. Chen, B. Zhu, F. Zhang, Y. Han, Z. Bo, *Angew. Chem.* **2008**, *120*, 6104–6107; *Angew. Chem. Int. Ed.* **2008**, *47*, 6015–6018; c) Z. Huang, S. K. Kang, M. Banno, T. Yamaguchi, D. Lee, C. Seok, E. Yashima, M. Lee, *Science* **2012**, *337*, 1521–1526.
- [11] a) S. S. Babu, S. Mahesh, K. K. Kartha, A. Ajayaghosh, *Chem. Asian J.* **2009**, *4*, 824–829; b) D. Dasgupta, S. Srinivasan, C. Rochas, A. Ajayaghosh, *J.-M. Guenet, Soft Matter* **2011**, *7*, 9311–9315.
- [12] K. Maeda, H. Mochizuki, K. Osato, E. Yashima, *Macromolecules* **2011**, *44*, 3217–3226.
- [13] T. H. Nguyen, R. J. Ansell, *Org. Biomol. Chem.* **2009**, *7*, 1211–1220.
- [14] S. Yu, W. Plunkett, M. Kim, L. Pu, *J. Am. Chem. Soc.* **2012**, *134*, 20282–20285.
- [15] a) J. Liu, Y. Feng, Z. X. Liu, Z. C. Yan, Y. M. He, C. Y. Liu, Q. H. Fan, *Chem. Asian J.* **2013**, *8*, 572–581; b) Y. W. Huang, B. G. Quan, Z. X. Wei, G. T. Liu, L. F. Sun, *J. Phys. Chem. C* **2009**, *113*, 3929–3933; c) G. T. Wang, J. B. Lin, X. K. Jiang, Z. T. Li, *Langmuir* **2009**, *25*, 8414–8418; d) X. D. Yu, Q. A. Liu, J. C. Wu, M. M. Zhang, X. H. Cao, S. Zhang, Q. Wang, L. M. Chen, T. Yi, *Chem. Eur. J.* **2010**, *16*, 9099–9106; e) P. Sahoo, D. K. Kumar, S. R. Raghavan, P. Dastidar, *Chem. Asian J.* **2011**, *6*, 1038–1047.
- [16] a) X. F. Zhu, Y. G. Li, P. F. Duan, M. H. Liu, *Chem. Eur. J.* **2010**, *16*, 8034–8040; b) P. F. Duan, Y. G. Li, L. C. Li, J. G. Deng, M. H. Liu, *J. Phys. Chem. B* **2011**, *115*, 3322–3329; c) P. F. Duan, X. F. Zhu, M. H. Liu, *Chem. Commun.* **2011**, *47*, 5569–5571; d) Q. X. Jin, L. Zhang, X. F. Zhu, P. F. Duan, M. H. Liu, *Chem. Eur. J.* **2012**, *18*, 4916–4922; e) X. F. Wang, P. F. Duan, M. H. Liu, *Chem. Commun.* **2012**, *48*, 7501–7503; f) Q. Jin, L. Zhang, M. Liu, *Chem. Eur. J.* **2013**, *19*, 9234–9241.
- [17] J. D. Luo, Z. L. Xie, J. W. Y. Lam, L. Cheng, H. Y. Chen, C. F. Qiu, H. S. Kwok, X. W. Zhan, Y. Q. Liu, D. B. Zhu, B. Z. Tang, *Chem. Commun.* **2001**, 1740–1741.
- [18] a) Z. Zhao, J. W. Y. Lam, B. Z. Tang, *Soft Matter* **2013**, *9*, 4564–4579; b) Y. L. Chen, Y. X. Lv, Y. Han, B. Zhu, F. Zhang, Z. S. Bo, C. Y. Liu, *Langmuir* **2009**, *25*, 8548–8555; c) P. Xue, R. Lu, G. Chen, Y. Zhang, H. Nomoto, M. Takafuji, H. Ihara, *Chem. Eur. J.* **2007**, *13*, 8231–8239; d) T. H. Kim, M. S. Choi, B. H. Sohn, S. Y. Park, W. S. Lyoo, T. S. Lee, *Chem. Commun.* **2008**, 2364–2366; e) C. Y. Bao, R. Lu, M. Jin, P. C. Xue, C. H. Tan, G. F. Liu, Y. Y. Zhao, *Org. Biomol. Chem.* **2005**, *3*, 2508–2512; f) S. Y. Li, L. M. He, F. Xiong, Y. Li, G. Q. Yang, *J. Phys. Chem. B* **2004**, *108*, 10887–10892.
- [19] D. L. Allara, R. G. Nuzzo, *Langmuir* **1985**, *1*, 45–52.
- [20] M. Jackson, H. H. Mantsch, *Can. J. Chem.* **1991**, *69*, 1639–1642.
- [21] H. Cao, Q. Z. Yuan, X. F. Zhu, Y. P. Zhao, M. H. Liu, *Langmuir* **2012**, *28*, 15410–15417.
- [22] P. F. Duan, L. Qin, X. F. Zhu, M. H. Liu, *Chem. Eur. J.* **2011**, *17*, 6389–6395.
- [23] a) Y. Che, X. Yang, S. Loser, L. Zang, *Nano Lett.* **2008**, *8*, 2219–2223; b) B.-P. Jiang, D.-S. Guo, Y. Liu, *J. Org. Chem.* **2010**, *75*, 7258–7264; c) H. Peng, L. Ding, T. Liu, X. Chen, L. Li, S. Yin, Y. Fang, *Chem. Asian J.* **2012**, *7*, 1576–1582; d) P. C. Xu, H. T. Yu, X. X. Li, *Anal. Chem.* **2011**, *83*, 3448–3454; e) B.-P. Jiang, D.-S. Guo, Y. Liu, *J. Org. Chem.* **2011**, *76*, 6101–6107.

Received: November 12, 2013  
Published online: January 21, 2014